Vibration analysis of thermally loaded isotropic and composite beam and plate structures

Journal of Thermal Stresses

ISSN: (Print) (Online) Journal homepage: https://www.tandfonline.com/loi/uths20

Vibration analysis of thermally loaded isotropic and composite beam and plate structures

R. Azzara, E. Carrera, M. Filippi & A. Pagani

To cite this article: R. Azzara, E. Carrera, M. Filippi & A. Pagani (2023) Vibration analysis of thermally loaded isotropic and composite beam and plate structures, Journal of Thermal Stresses, 46:5, 369-386, DOI: 10.1080/01495739.2023.2188399

To link to this article: https://doi.org/10.1080/01495739.2023.2188399

Published online: 22 Mar 2023.

JOURNAL OF THERMAL STRESSES
2023, VOL. 46, NO. 5, 369–386
https://doi.org/10.1080/01495739.2023.2188399

Taylor & Francis
Taylor & Francis Group

Vibration analysis of thermally loaded isotropic and composite beam and plate structures

R. Azzara[a], E. Carrera[a,b], M. Filippi[a], and A. Pagani[a]

[a]Department of Mechanical and Aerospace Engineering, Politecnico di Torino, Torino, Italy; [b]Department of Mechanical Engineering, College of Engineering, Prince Mohammad Bin Fahd University, Kingdom of Saudi Arabia

ABSTRACT

This work proposed the use of the Carrera Unified Formulation (CUF) for the vibration and buckling analysis of structures subjected to thermal loads. In detail, the variation of natural frequencies for progressively large thermal loads is investigated. Here, particular attention is focused on the study of buckling thermal loads as degenerate cases of the vibration analysis and on the mode aberration caused by thermal stresses. From this standpoint, the use of CUF for the development of high-order beam and plate models is fundamental. Indeed, Lagrange-like (LE) polynomials are considered for developing the kinematic expansion and Layerwise (LW) theories are employed to characterize the complex phenomena that may appear in composite structures. A linearized formulation to study the natural frequencies variation as a function of the progressive increasing thermal loadings is adopted. Different isotropic and laminated composite structures have been analyzed and compared with the Abaqus solution to validate the presented methodology and provide some benchmark solutions. In addition, a parametric study was conducted to evaluate the stacking sequence and thickness effect in the vibration modes and thermal buckling loads. The results document the excellent accuracy and reliability of the presented methodology and show the potentialities of this numerical tool able to analyze cases that are difficult to study experimentally.

ARTICLE HISTORY
Received 21 July 2022
Accepted 12 February 2023

KEYWORDS
Beam model; Carrera Unified Formulation; Layerwise; mode aberration; plate model; thermal buckling; vibration

1. Introduction

Aerospace structures are usually required to operate under particular conditions that take into account thermal loads. From a structural point of view, the question is whether the variations in the temperature during the lifetime of an aircraft are sufficient to compromise its integrity. Some key parameters of the thermal load are changes in average temperature and temperature differentials. Thin-walled structures, typically adopted in aeronautical engineering, are highly efficient in terms of mass but also vulnerable to instability phenomena, which can be exploited to improve the structural performance [1]. The buckling of structures subjected to mechanical loading has been widely examined over the years. On the other hand, thermal buckling was avoided and, for this reason, the available literature on thermomechanical vibration and thermal buckling analysis is not extensive [2]. However, a good investigation of thermomechanically buckled states can help

CONTACT R. Azzara rodolfo.azzara@polito.it Department of Mechanical and Aerospace Engineering, Politecnico di Torino Corso Duca degli Abruzzi 24, 10129 Torino, Italy.

structural designers to identify potential advantage opportunities, make better choices and eventually contribute to better future designs. In this context, new research trends have been focused on new conceptions about buckling predictions and natural frequencies characterization [3–5].

The importance of thermal effect on structures emerged with the supersonic flight [6, 7]. Over the years, the focus has evolved, ranging from innovative structural configurations and geometries to the introduction of next-generation aerospace materials. Therefore, thermal instability analysis began to attract interest among many scientists and researchers. For example, Thornton [8] provided various progresses on thermal analyzes on structures from supersonic flight to the current research. Several experiments in heated composite plate structures were performed by Gutiérrez Álvarez and Bisagni [9]. Murphy and Ferreira [10] carried out thermal buckling analyses for clamped, rectangular plates by considering energy considerations and experimental investigations. Various thermal buckling analyses of functionally graded plate structures using analytical formulations were carried out by Javaheri and Eslami [11]. Pradeep et al. [12] provided vibration and thermal buckling analysis of different composite sandwich beam structures with viscoelastic core. Thermal bucking analyses of laminated composite plate structures were investigated by Prabhu and Dhanaraj [13], in which a finite element method based on the Reissner–Mindlin first-order shear deformation theory is employed. Bhagat and Yeyaraj [14] carried out various experiment tests to evaluate the effect of nonuniform temperature distributions on the thermal buckling of shell structures. Jeyaraj [15] provided free vibration and buckling analysis of metallic plates with thermal pre-stress. For completeness, readers are referred to [16–19] for other interesting work about thermal buckling analysis. The amount of work available in the literature on experiments on thermal buckling prediction through vibration data is not, however, large. Especially, the topic of mode jumping or mode change through mechanically or thermally induced instability has been addressed on limited occasions [20].

To prove the feasibility of particular phenomena under different loading types, experimental tests are an essential milestone. However, one of the researchers' goals over the years has been to reduce both the time and cost of operations of these complex studies. One of the effective approaches to do this is to adopt nondestructive experimental tests to compute the critical buckling load of structures. One of the most used nondestructive methods is represented by the Vibration Correlation Technique (VCT) [21, 22]. The latter computes the critical load and the equivalent boundary conditions by interpolating the natural frequencies of the structures for progressively rising applied loadings without reaching the point of instability. The first experimental VCT studies were data from the 1950s, with the analyses conducted by Lurie [23], Meier [24], and Chu [25]. Over the years, several approaches have been formulated to obtain reliable results of buckling prediction and natural frequency variation. For example, a new relation between the natural frequencies and the applied loadings was presented by Souza and Assaid [26]. Arbelo et al. [27, 28] implemented a modified-VCT based on the considerations made by Souza et al. The literature on VCT studies of structures subjected to mechanical loads is vast, whereas the one considering thermal loadings is limited. Since a complete review of the VCT formulations is not the purpose of this article, the reader is referred to the book written by Abramovich [29] for interesting test setup and results.

The goal of the present research is to show a new numerical approach able to study critical buckling behaviors, characterize natural frequencies variation, provide a means to verify VCT results, and present benchmark solutions of isotropic and laminated composite beam and plate structures subjected to uniform thermal loadings. The effect of the temperature changes on the buckling loads and natural frequencies were investigated, including a parametric study conducted on the stacking sequence and thickness.

The presented methodology is formulated in the Carrera Unified Formulation (CUF) domain, see [30]. One of the main advantages of this formulation is that classical to high-order models can be implemented simply and automatically. In fact, the governing equations and the relative

finite element (FE) arrays of the one-dimensional (1D) and two-dimensional (2D) theories are expressed in terms of Fundamental Nuclei (FNs). In this article, both Lagrange-like (LE) and Taylor-like (TE) polynomials are considered. When laminated composite structures are studied, the Layerwise kinematic [31, 32] is adopted. Note that CUF was already successfully used in many engineering fields [32–35], and in the present work, it is adopted to perform vibration analysis of thermal pre-stress structures.

This manuscript is structured as follows: (i) first, the methodology adopted in this work to perform vibration analysis for thermally loaded isotropic and composite structures is provided in Section 2; (iii) then, numerical solutions in terms of natural frequencies variation and buckling loads are discussed in Section 3, including the comparison with the Abaqus solution; (iv) finally, Section 4 summarizes the main conclusions.

2. Vibration analysis for thermally loaded structures

Considering a generic continuous body, each of its points can be subject to displacements in the three directions of space according to a Cartesian reference system. In this work, both isotropic and composite beam and plate structures were studied. For clarity, the following discussion is carried out considering a laminated composite beam structure, in which k stands for the kth layer. Although derivation is carried out for beams, it should be highlighted that similar relations hold for plate models. Consequently, the displacement, strain and stress fields are introduced as follows:

$$\begin{aligned} \boldsymbol{u}^k &= \{u_x^k \;\; u_y^k \;\; u_z^k\}^{\mathrm{T}} \\ \boldsymbol{\epsilon}^k &= \{\varepsilon_{xx}^k \;\; \varepsilon_{yy}^k \;\; \varepsilon_{zz}^k \;\; \varepsilon_{xz}^k \;\; \varepsilon_{yz}^k \;\; \varepsilon_{xy}^k\}^{\mathrm{T}} \\ \boldsymbol{\sigma}^k &= \{\sigma_{xx}^k \;\; \sigma_{yy}^k \;\; \sigma_{zz}^k \;\; \sigma_{xz}^k \;\; \sigma_{yz}^k \;\; \sigma_{xy}^k\}^{\mathrm{T}} \end{aligned} \tag{1}$$

In the case of small displacements, linear strain–displacement relation is considered. It reads:

$$\boldsymbol{\epsilon}^k = \boldsymbol{b}\boldsymbol{u}^k \tag{2}$$

in which $\boldsymbol{\epsilon}^k$ is the full Green-Lagrange strain tensor and $\boldsymbol{b}$ represents the nonlinear differential operator.

Hooke's law expresses the physical relationship between the stresses and deformation components by means of the material elastic matrix for orthotropic materials $\boldsymbol{C}^k$ [36, 37].

$$\boldsymbol{\sigma}^k = \boldsymbol{C}^k\boldsymbol{\epsilon}^k \tag{3}$$

According to 1D CUF, the 3D displacement field in the dynamic case is an expansion of generic functions $F_\tau(x,z)$ for the generalized displacement vector $\boldsymbol{u}_\tau(y;t)$, which are functions of the coordinate y laying along the main structural dimension. Hence:

$$\boldsymbol{u}^k(x,y,z;t) = F_\tau^k(x,z)\boldsymbol{u}_\tau^k(y;t) \qquad \tau = 1,\ldots,M \tag{4}$$

where t indicates time, M is the number of the terms adopted in the expansion and the repeated subscript τ denotes summation. The choice of F_τ determines the class of the 1D and 2D CUF models. LE CUF models as used in the present research can be found in [36]. In detail, the nine-point (L9) Lagrange polynomials in the cross-section for beam model and the four-node (LD3) Lagrange expansion functions in the z direction for plates were used in the following analyses. For brevity, the interested reader is referred to [30, 38] for a detailed explanation of the mathematical derivation of the 1D and 2D FE formulation in the CUF domain.

Independently of the selected beam model kinematics, the generalized displacements can be approximated along the beam axis by introducing the Finite Element Method (FEM) and using the shape functions $N_i(y)$.

$$\boldsymbol{u}_\tau^k(y;t) = N_i(y)\boldsymbol{q}_{\tau i}^k(t), \qquad i = 1, ..., N_n \tag{5}$$

where $\boldsymbol{q}_{\tau i}$ is the vector of the unknown nodal variables, N_n indicates the number of nodes per element and i represents summation. For clarity, the four-node (B4) cubic beam elements and the classical 2D nine-node (Q9) quadratic finite elements are adopted in this work as shape functions [39]. By considering the strain (ϵ) and having the CUF (Eq. (4)) and FEM (Eq. (5)) relations into Eq. (2), the strain vector can be expressed in algebraic form as:

$$\boldsymbol{\epsilon}^k = \boldsymbol{b}(F_\tau^k N_i)\boldsymbol{q}_{\tau i}^k = \boldsymbol{B}^k \boldsymbol{q}_{\tau i}^k \tag{6}$$

For brevity, this nonlinear matrix $\boldsymbol{B}^k$ can be found in [40].

In the linear thermoelasticity, the elastic strain vector $\boldsymbol{\epsilon}_e^k$ is equal to:

$$\boldsymbol{\epsilon}_e^k = \boldsymbol{\epsilon}^k - \boldsymbol{\epsilon}_T^k \tag{7}$$

where $\boldsymbol{\epsilon}^k$ represents the total strain vector and $\boldsymbol{\epsilon}_T^k$ is the strain vector due to the temperature change $\Delta T = T - T_0$, that is expressed as follows:

$$\boldsymbol{\epsilon}_T^k = \boldsymbol{\alpha}^k \Delta T \tag{8}$$

in which T_0 indicates the reference temperature and $\boldsymbol{\alpha}$ denotes the linear thermal expansion coefficients vector. Consequently, it is possible to define a new constitutive law given by:

$$\boldsymbol{\sigma}^k = \boldsymbol{\sigma}_H^k - \boldsymbol{\sigma}_T^k = \boldsymbol{C}^k \boldsymbol{\epsilon}^k - \boldsymbol{\beta}^k \Delta T \tag{9}$$

in which the subscript H indicates the quantities relating to Hooke's law, whereas T those relating to thermal deformation. In Eq. (9), $\boldsymbol{\beta}^k$ represents the vector of the stress–temperature moduli. It reads:

$$\boldsymbol{\beta}^k = \boldsymbol{C}^k \boldsymbol{\alpha}^k \tag{10}$$

The governing equations of the free vibrations around trivial equilibrium states are written adopting the principle of virtual work. Namely:

$$\delta L_{\text{int}} = -\delta L_{\text{ine}} \tag{11}$$

in which δL_{int} stands for the virtual variation of the internal strain energy and δL_{ine} is the virtual variation of the inertial loads. They are expressed as follows:

$$\begin{aligned}
\delta L_{\text{int}} &= \int_V \delta \boldsymbol{\epsilon}_e^{k\mathrm{T}} (\boldsymbol{C}^k \boldsymbol{\epsilon}^k - \boldsymbol{\beta}^k \Delta T)\, dV = \int_V \delta \boldsymbol{q}_{sj}^{k\mathrm{T}} \boldsymbol{B}^{k\mathrm{T}} (\boldsymbol{C}^k \boldsymbol{B}^k \boldsymbol{q}_{\tau i}^k - \boldsymbol{\beta}^k \Delta T)\, dV = \\
&= \int_V \delta \boldsymbol{q}_{sj}^{k\mathrm{T}} \boldsymbol{B}^{k\mathrm{T}} (\boldsymbol{C}^k \boldsymbol{B}^k \boldsymbol{q}_{\tau i}^k)\, dV - \int_V \delta \boldsymbol{q}_{sj}^{k\mathrm{T}} \boldsymbol{B}^{k\mathrm{T}} (\boldsymbol{\beta}^k \Delta T)\, dV = \\
&= \delta \boldsymbol{q}_{sj}^{k\mathrm{T}} \boldsymbol{K}_S^{ij\tau s k} \boldsymbol{q}_{\tau i}^k - \delta \boldsymbol{q}_{sj}^{k\mathrm{T}} \boldsymbol{F}_{T\,sj}^k
\end{aligned} \tag{12}$$

$$\delta L_{ine} = \int_V \delta \boldsymbol{u}^{k\mathrm{T}} \rho \boldsymbol{u}''^{\,\mathrm{k}}\, dV = \delta \boldsymbol{q}_{sj}^{k\mathrm{T}} \boldsymbol{M}^{ij\tau s k}\, \boldsymbol{q}''^{\,\mathrm{k}}_{\tau i}$$

where V denotes the volume, the $\boldsymbol{K}_S^{ij\tau sk}$ represents the secant stiffness matrix, $\boldsymbol{F}_{T_{sj}}^{k}$ is the thermal load vector, that is an artificial forces for modeling thermal expansion, $\boldsymbol{M}^{ij\tau s^k}$ is the mass matrix, that is assumed to be linear, ρ denotes the density, $\ddot{\boldsymbol{q}}_{\tau i}^{\mathrm{k}}$ stands for the nodal acceleration vector and the dot indicates $\delta/\delta t$. The superscripts i, j, τ, s are the four indexes exploited to assemble the matrices.

As in this research the goal is to study the vibrations of structures subjected to initial displacements and pre-stress, Eq. (11) has to be linearized around trivial equilibrium states. Therefore, the linearization of the virtual variation of the internal strain energy holds:

$$\delta(\delta L_{int}) = \int_V \delta(\delta \boldsymbol{\epsilon}_e^{k\mathrm{T}} \boldsymbol{\sigma}^k)\, dV = \int_V \delta \boldsymbol{\epsilon}_e^{k\mathrm{T}} \delta \boldsymbol{\sigma}^k\, dV + \int_V \delta(\delta \boldsymbol{\epsilon}_e^{k\mathrm{T}}) \boldsymbol{\sigma}^k\, dV = \delta \boldsymbol{q}_{sj}^{k\mathrm{T}} \boldsymbol{K}_T^{ij\tau sk} \delta \boldsymbol{q}_{\tau i}^{k} \tag{13}$$

in which $\boldsymbol{K}_T^{ij\tau s^k}$ represents the tangent stiffness matrix. In the case of small rotations and linear pre-buckling, $\boldsymbol{K}_T^{ij\tau s^k}$ can be approximated as the sum of the linear stiffness ($\boldsymbol{K}_0^{ij\tau s^k} = \boldsymbol{K}_S^{ij\tau s^k}(\boldsymbol{q}_{\tau i}^{k} = 0)$) and the geometric (pre-stress) contribution ($\boldsymbol{K}_\sigma^{ij\tau s^k}$) [41, 42].

$$\boldsymbol{K}_T^{ij\tau sk} \approx \boldsymbol{K}_0^{ij\tau sk} + \lambda \boldsymbol{K}_\sigma^{ij\tau s^k} \tag{14}$$

where λ is the progressively increasing load factor. It is important to underline that, in this case, the $\boldsymbol{K}_\sigma^{ij\tau sk}$ matrix refers to the linear contributions of stress ($\boldsymbol{\sigma}_{lin}^{k}$). Once the $\boldsymbol{K}_T^{ij\tau sk}$ is calculated for each ply of the laminated structure, an LW assembly procedure is adopted according to [43, 44] to obtain the global assembled tangent stiffness matrix ($\boldsymbol{K}_T$).

The introduction of thermal loads determines a new definition of the geometric stiffness matrix $\boldsymbol{K}_\sigma^{ij\tau sk}$ due to the new constitutive equation reported in Eq. (9). For reasons of clarity, superscripts are omitted in the following relations. After simple manipulations, the geometric stiffness matrix is obtained as follows:

$$\begin{aligned} \int_V \delta(\delta \boldsymbol{\epsilon}^{k\mathrm{T}}) \boldsymbol{\sigma}_{lin}^{k}\, dV = \int_V \delta \boldsymbol{q}_{sj}^{k\mathrm{T}} \boldsymbol{B}_{nl}^{*\,k\mathrm{T}} \boldsymbol{\sigma}_{lin}^{k}\, dV = \delta \boldsymbol{q}_{sj}^{k\mathrm{T}} \int_V \boldsymbol{B}_{nl}^{*\,k\mathrm{T}} \boldsymbol{C}^k \boldsymbol{\epsilon}^k\, dV\, \delta \boldsymbol{q}_{\tau i}^{k} + \\ - \delta \boldsymbol{q}_{sj}^{k\mathrm{T}} \int_V \boldsymbol{B}_{nl}^{*\,k\mathrm{T}} \boldsymbol{\beta}^k \Delta T\, dV\, \delta \boldsymbol{q}_{\tau i}^{k} = \delta \boldsymbol{q}_{sj}^{k\mathrm{T}} \boldsymbol{K}_\sigma^k \delta \boldsymbol{q}_{\tau i}^{k} - \delta \boldsymbol{q}_{sj}^{k\mathrm{T}} \boldsymbol{K}_{\sigma T}^k \delta \boldsymbol{q}_{\tau i}^{k} \end{aligned} \tag{15}$$

in which the $\boldsymbol{K}_{\sigma T}^{k}$ represents the new term of the geometric stiffness matrix due to the thermal contribution. For clarity, it should be noted once again that only linear contributions are taken into account. Interested readers can find the complete expression of the $\boldsymbol{B}_{nl}^{*\,k}$ and a detailed description of mathematical operations in [40].

Finally, by assuming harmonic motion around quasi-static equilibrium states, Eq. (11) has the form of a linear eigenvalue problem:

$$(\boldsymbol{K}_T - \omega^2 \boldsymbol{M})\boldsymbol{q} = 0 \tag{16}$$

where $\boldsymbol{M}$ represents the global assembled mass matrix, ω indicates the natural frequency and $\boldsymbol{q}$ denotes the eigenvector.

For the sake of clarity, the resolution procedure of the proposed approach is summarized in the following steps:

- First, the static geometrical nonlinear problem is solved using the Newton–Raphson method based on the arc-length approach.
- Once the nonlinear equilibrium curve is computed, the tangent stiffness matrix is obtained in each states of interest.

- Then, by linearizing the equation of motion and assuming harmonic displacement,

$$\delta \boldsymbol{q}_{\tau i}(t) = \delta \tilde{\boldsymbol{q}}_{\tau i} e^{i\omega t}$$
$$\delta \ddot{\boldsymbol{q}}_{\tau i}(t) = -\omega^2 \delta \tilde{\boldsymbol{q}}_{\tau i} e^{i\omega t} \tag{17}$$

- the equations of motion is simplified into a linear eigenvalues problem from which it is possible to evaluate natural frequencies and mode shapes.
- For the sake of clarity, it is important to underline how the nonlinear vibrations exhibit low amplitudes and small increment of amplitudes during the determination of the nonlinear vibration modes are considered; consequently, it is legitimate to use a linearization around the state of equilibrium for the resolution of the problem.

3. Numerical examples

This section provides a numerical linearized approach to perform vibration-buckling investigations of metallic and laminated beam and plate structures subjected to thermal loadings given by a uniform variation of the temperature ΔT on the entire model. The critical buckling loads and the natural frequencies variation with progressively higher thermal loadings of several structures are analyzed. The solutions are compared with results obtained using the commercial code Abaqus to prove the validity of the presented methodology. For the following analyses, clamped boundary conditions are adopted. Given the thermal loads and boundary conditions considered, it is possible to predict the generation of compressive stresses due to the tendency of the structures to expand as the temperature increases, a tendency which is, however, prevented by the constraint conditions.

3.1. Isotropic beam

The first numerical assessment consists of an isotropic square cross-section beam structure subjected to thermal loadings. Two different configurations, $L/h = 10$ and $L/h = 100$, are considered. In detail, the beam, illustrated in Figure 1, has the length L equal to 1 m, $a = 0.1$ m/0.01 m and $h = 0.1$ m/0.01 m. The elastic structure was made of aluminum with Young's modulus, Poisson's ratio, density and linear thermal expansion coefficient equal to $E = 73$ GPa, $\nu = 0.34$, $\rho = 2700\,\mathrm{kg/m^3}$, and $\alpha = 25 \times 10^{-6}\ ^\circ\mathrm{C}^{-1}$, respectively.

After a convergence analysis not displayed here for the sake of brevity, the mathematical model consists of four nine-point Lagrange polynomials (L9) on the cross-section (x – z) and ten four-node cubic (B4) beam finite elements along the y-axis. The number of degrees of freedom is, therefore, 2325. The accuracy of the discretization chosen, according to the CUF theory, was verified by making a comparison with the results of the modal analysis obtained through the commercial FE software Abaqus (ABQ) [45] using $10 \times 2 \times 2$ C3D20R solid elements, see Table 1.

The characteristics first three free vibration mode shapes of both thick and thin isotropic beam structures are provided in Figure 2.

Generally speaking, the application of a thermal load to a structure in particular constraint conditions involves the rise of a state of tension generated by the expansion of the structure.

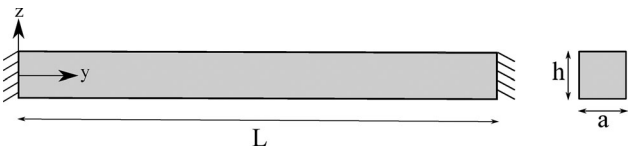

Figure 1. Geometry and boundary condition of the clamped-clamped beam structure subjected to thermal loadings.

Table 1. Comparison between the present methodology and the Abaqus solution.

Model	I flexural mode	II flexural mode	I torsional mode
CUF LE9 (Hz)	508.85	1,303.07	1,476.05
Abaqus Hex20 (Hz)	509.01	1,303.90	1,471.52

Isotropic beam ($L/h = 10$).

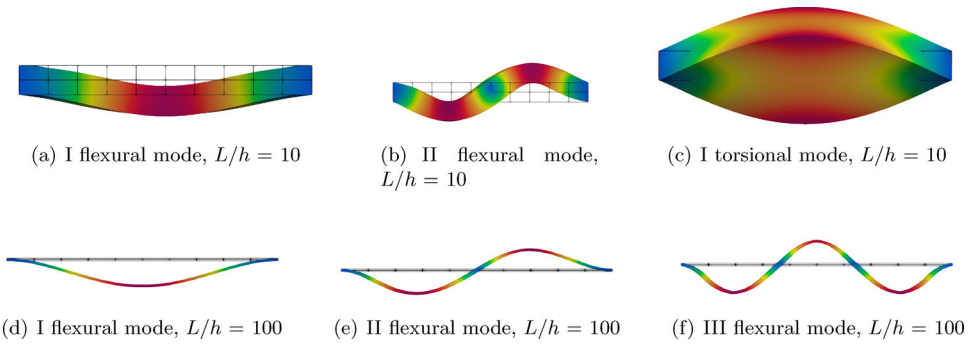

(a) I flexural mode, $L/h = 10$ (b) II flexural mode, $L/h = 10$ (c) I torsional mode, $L/h = 10$

(d) I flexural mode, $L/h = 100$ (e) II flexural mode, $L/h = 100$ (f) III flexural mode, $L/h = 100$

Figure 2. Characteristics first three free vibration mode shapes for clamped-clamped isotropic beams.

Especially considering the boundary conditions of the present beam with both edges clamped, the application of a thermal load, due to a uniform variation of the temperature on the whole model, leads to a state of compression stress that can lead to buckling of the structure.

Figure 3 plots the comparison between the natural frequencies variation for progressively increasing thermal loadings computed via the present methodology and Abaqus. The results obtained show a good correlation with the Abaqus ones, allowing one to predict the critical buckling load and evaluate the natural frequencies variation with high reliability. Particularly, the graphs suggest that instability phenomena occur for a thermal load corresponding to 1139.03 °C for the case of the thick beam and 13.04 °C for the slender one. Regarding the thick structure, see Figure 3a, given the very high ΔT_{cr} value obtained for the beam in an isotropic material, similar to an aluminum alloy, in this case, the instability configuration will never be reached. However, it is possible to have a considerable, albeit secondary, effect when considering a more complex load environment where the thermal load is only one of the contributors.

3.2. Laminated composite [0°/90°/0°] beam

The second analysis case deals with a laminated composite beam structure subjected to thermal loadings. The same geometrical data are used as in the previous example. The lamination sequence considered is [0°/90°/0°]. The material properties of this laminated structure involves $E_1 = 144.8\,\text{GPa}$, $E_2 = E_3 = 9.65\,\text{GPa}$, $\nu_{12} = 0.3$, $G_{12} = G_{13} = 4.14\,\text{GPa}$, $G_{23} = 3.45\,\text{GPa}$, $\rho = 1450\,\text{kg/m}^3$, $\alpha_{11} = -2.6279 \times 10^{-7}\text{°C}^{-1}$ and $\alpha_{12} = 30.535 \times 10^{-6}\text{°C}^{-1}$. The convergent model for this beam structure is reached by employing at least ten B4 finite elements along the beam-axis and two Q9 for each layer.

Table 2 shows the comparison between the present formulation and Abaqus solution for the first six free natural frequencies. Furthermore, the mode shapes of both thick and thin laminated composite beam structures are depicted in Figure 4.

Also, in this case, the instability behavior of the composite beam under thermal loadings given by the uniform variation of the temperature ΔT was confirmed by the frequency trend of the beam modes with respect to the thermal load, see Figure 5. The current results were compared with those obtained with Abaqus. The comparisons revealed a perfect agreement between the two approaches within the considered thermal load interval.

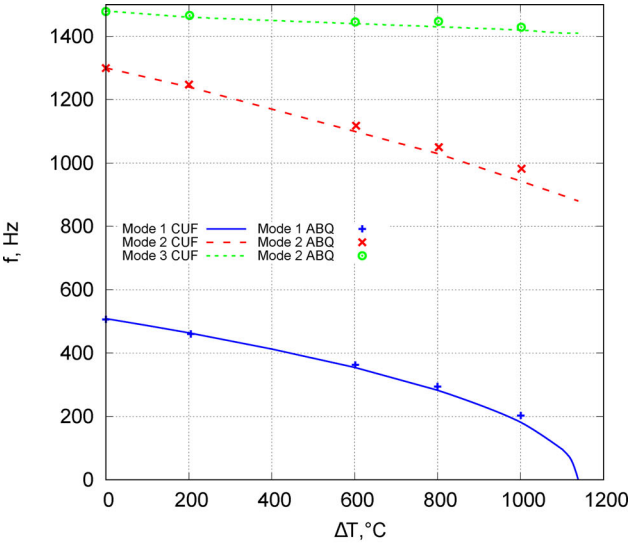

(a) $L/h = 10$

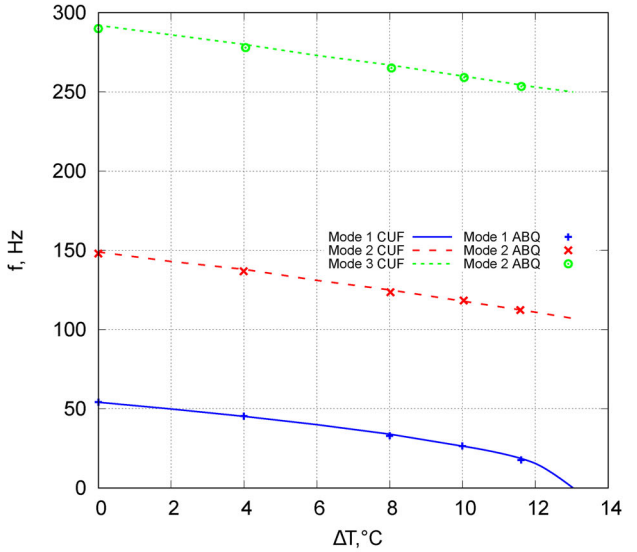

(b) $L/h = 100$

Figure 3. Natural frequency variation versus thermal loadings for the isotropic beam.

Table 2. Comparison between the present methodology and the Abaqus solution.

	CUF LE9 (Hz)	Abaqus Hex20 (Hz)
I flexural mode *xy*-plane	571.35	571.83
I flexural mode *yz*-plane	605.34	605.16
I torsional mode	773.82	773.20
II flexural mode *xy*-plane	1,234.41	1,235.90
II flexural mode *yz*-plane	1,270.84	1,273.80
II torsional mode	1,551.99	1,552.10

Laminated composite [0°/90°/0°] beam. $L/h = 10$.

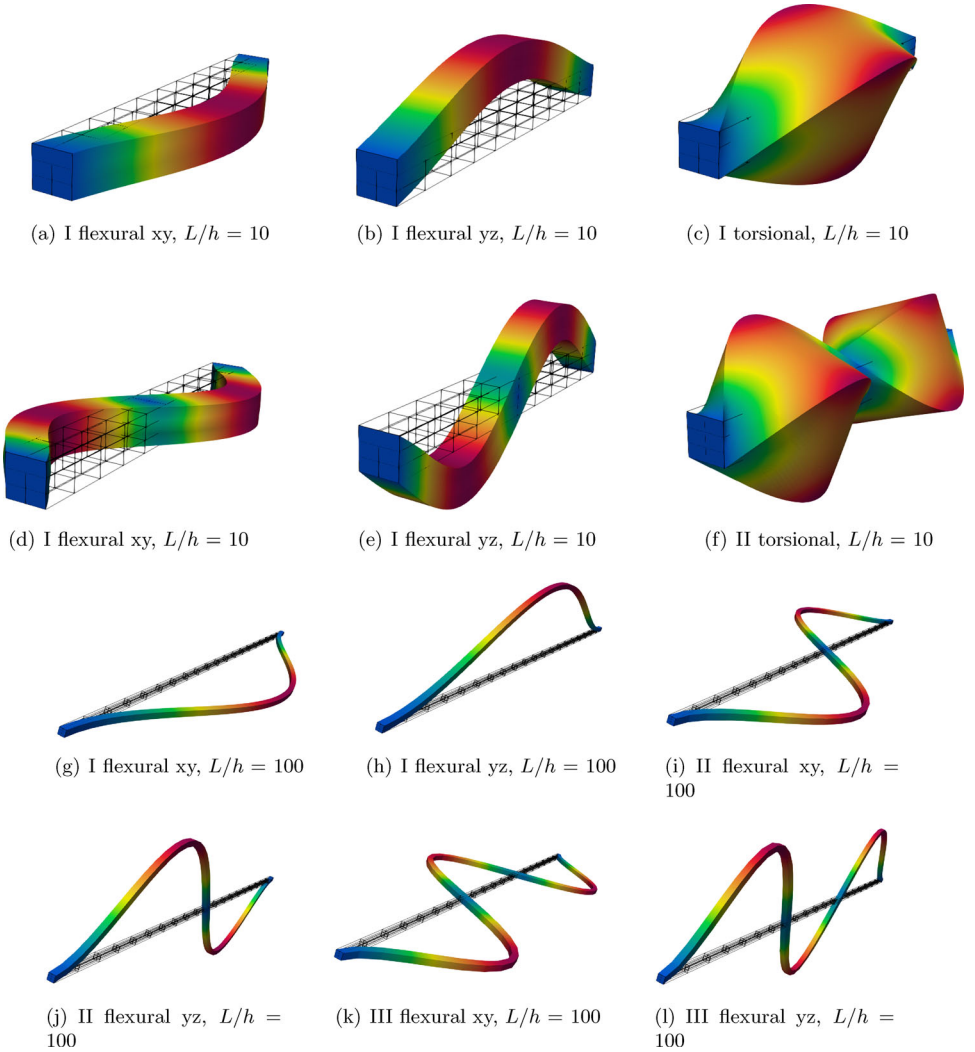

(a) I flexural xy, $L/h = 10$ (b) I flexural yz, $L/h = 10$ (c) I torsional, $L/h = 10$

(d) I flexural xy, $L/h = 10$ (e) I flexural yz, $L/h = 10$ (f) II torsional, $L/h = 10$

(g) I flexural xy, $L/h = 100$ (h) I flexural yz, $L/h = 100$ (i) II flexural xy, $L/h = 100$

(j) II flexural yz, $L/h = 100$ (k) III flexural xy, $L/h = 100$ (l) III flexural yz, $L/h = 100$

Figure 4. Characteristics first three free vibration mode shapes for clamped-clamped laminated composite [0°/90°/0°] thick and thin beams.

3.3. Isotropic plate

An isotropic square plate structure subjected to thermal loadings is investigated in the following analysis case. Figure 6 illustrates the structure geometry, with $a = 1$ m, $h = 0.01$ m, and the boundary conditions used. The material data are the following: $E = 73$ GPa, $\nu = 0.34$, $\rho = 2700$ kg/m^3 and $\alpha = 25 \times 10^{-6\circ}\text{C}^{-1}$. The mathematical model consisted of 10×10 Q9 finite elements over the *xy*-plane, while the kinematic theory adopted along the thickness direction is only one LD2. Therefore, the number of degrees of freedom is 3969.

The values of the first four free vibration modes obtained using the CUF and Abaqus are tabulated in Table 3, whereas the mode shapes are depicted in Figure 7. For clarity, 10×10 S8R shell elements are adopted in the Abaqus model.

Figure 8 shows the natural frequencies variation versus increasing thermal loadings via the present linearized approach, including the comparison with the Abaqus solution. The graph shows that the first instability mode of the isotropic plate with all edges clamped, corresponding to a uniform temperature variation $\Delta T_{\text{cr}} = 13.16\,^{\circ}\text{C}$, coincides with the vibrational mode (1,1).

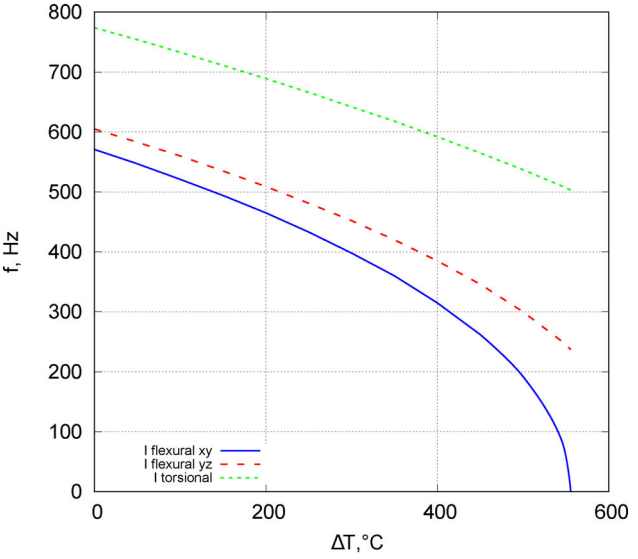

(a) $L/h = 10$

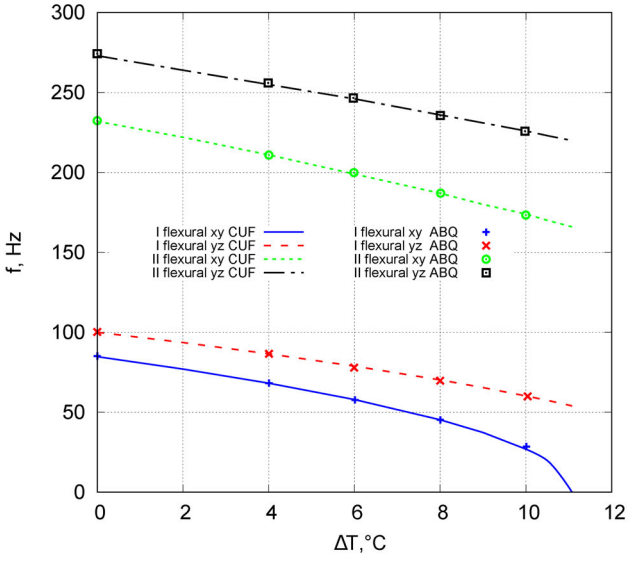

(b) $L/h = 100$

Figure 5. Natural frequency variation versus thermal loadings for the laminated composite [0°/90°/0°] beam.

3.4. Laminated composite plate

As a final example, a laminated composite plate structure under thermal loadings is analyzed. This plate model has the same geometric data as the previous case. The material data of the present plate structure are the following: $E_1 = 144.8\,\text{GPa}$, $E_2 = E_3 = 9.65\,\text{GPa}$, $\nu_{12} = 0.3$, $G_{12} = G_{13} = 4.14\,\text{GPa}$, $G_{23} = 3.45\,\text{GPa}$, $\rho = 1450\,\text{kg/m}^3$, $\alpha_{11} = -2.6279 \times 10^{-7\circ}\text{C}^{-1}$ and $\alpha_{12} = 30.535 \times 10^{-6\circ}\text{C}^{-1}$. The structure is modeled adopting 10×10 Q9 for the in-plane mesh approximation, whereas only one LD3 is used in each layer in the z-direction.

First, the dynamic behavior of the composite plate considering $a/h = 100$ and three-layer with [0°/90°/0°] staking sequence is investigated. Then, a parametric study based on the variation of the lamination sequence and thickness of the plate is performed.

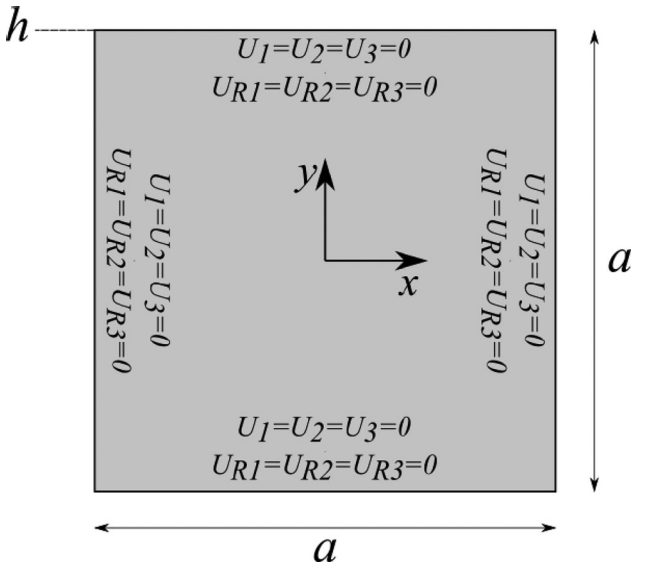

Figure 6. Geometry and boundary condition of the clamped isotropic plate structure ($a/h = 100$) subjected to thermal loadings.

Table 3. Comparison between the present methodology and the Abaqus solution

Model	Mode (1,1)	Mode (2,1)/(1,2)	Mode (2,2)
CUF (Hz)	93.89	194.90	287.01
Abaqus S8R (Hz)	91.40	186.47	275.77

Isotropic plate ($a/h = 100$).

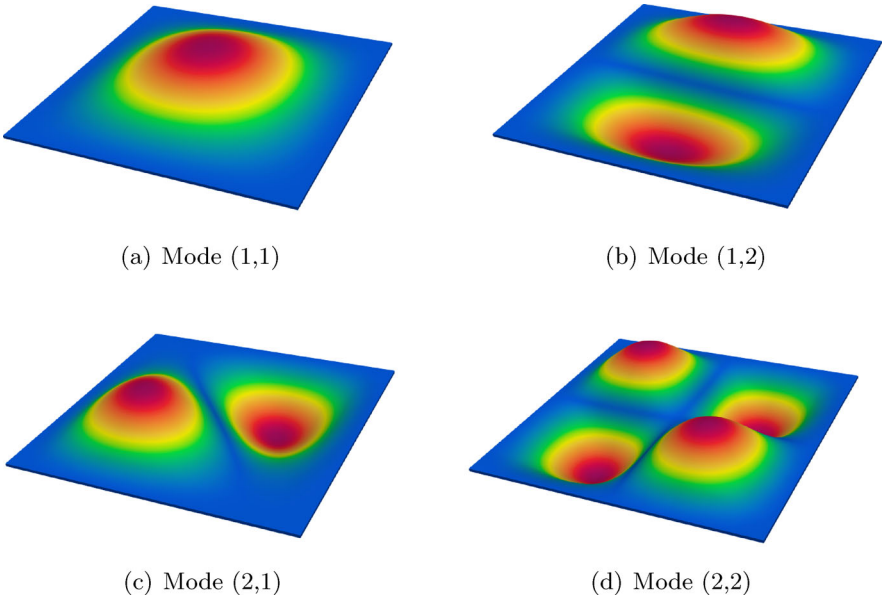

Figure 7. Characteristics first four free vibration mode shapes for the clamped isotropic plate ($a/h = 100$).

In Table 4 and Figure 9, the natural frequencies and mode shapes of the first five vibration modes are provided, respectively.

Figure 10 shows the comparison between the natural frequencies variation for progressively increasing thermal loadings obtained via the present linearized approach and the Abaqus solution.

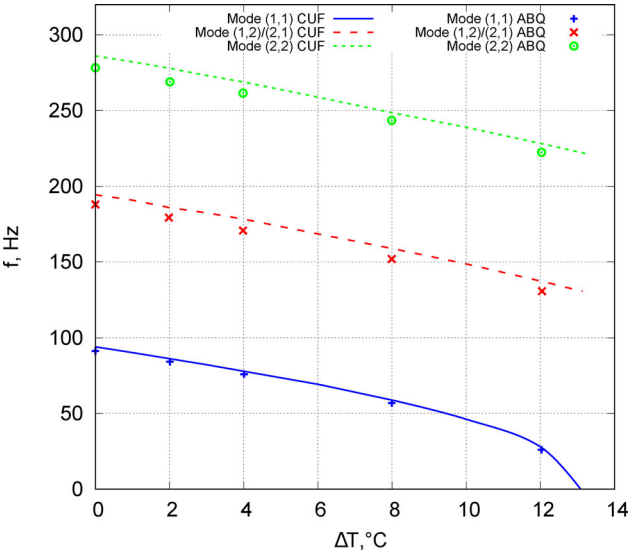

Figure 8. Natural frequency variation versus thermal loadings for the isotropic plate ($a/h = 100$).

Table 4. Comparison between the present methodology and the Abaqus solution.

Model	Mode (1,1)	Mode (2,1)	Mode (3,1)	Mode (1,2)	Mode (2,2)
CUF (Hz)	108.67	144.30	222.98	283.06	304.53
Abaqus S8R (Hz)	107.76	141.37	212.54	278.78	299.43

Laminated composite [0°/90°/0°] plate ($a/h = 100$).

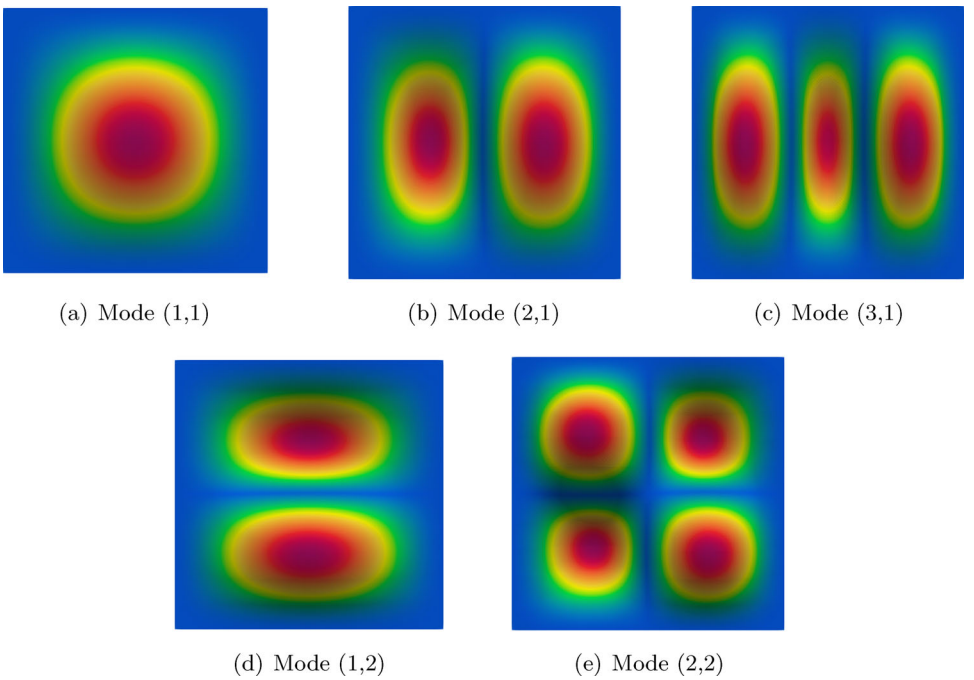

Figure 9. Characteristics first five free vibration mode shapes for the laminated composite [0°/90°/0°] plate ($a/h = 100$).

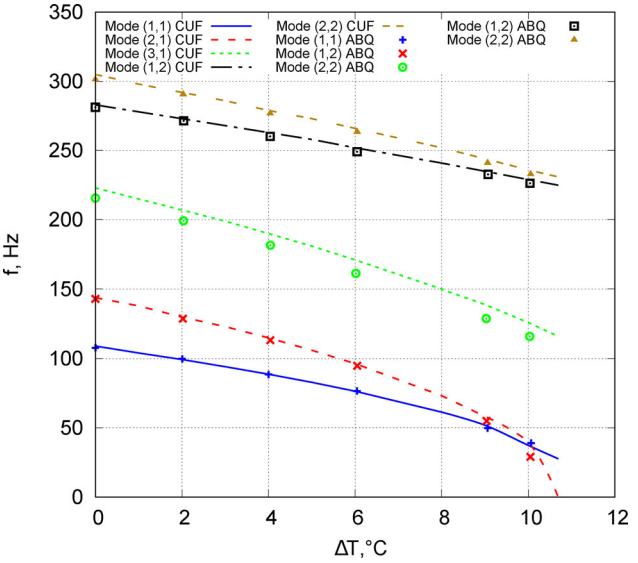

Figure 10. Natural frequency variation versus thermal loadings for the laminated composite [0°/90°/0°] plate ($a/h = 100$).

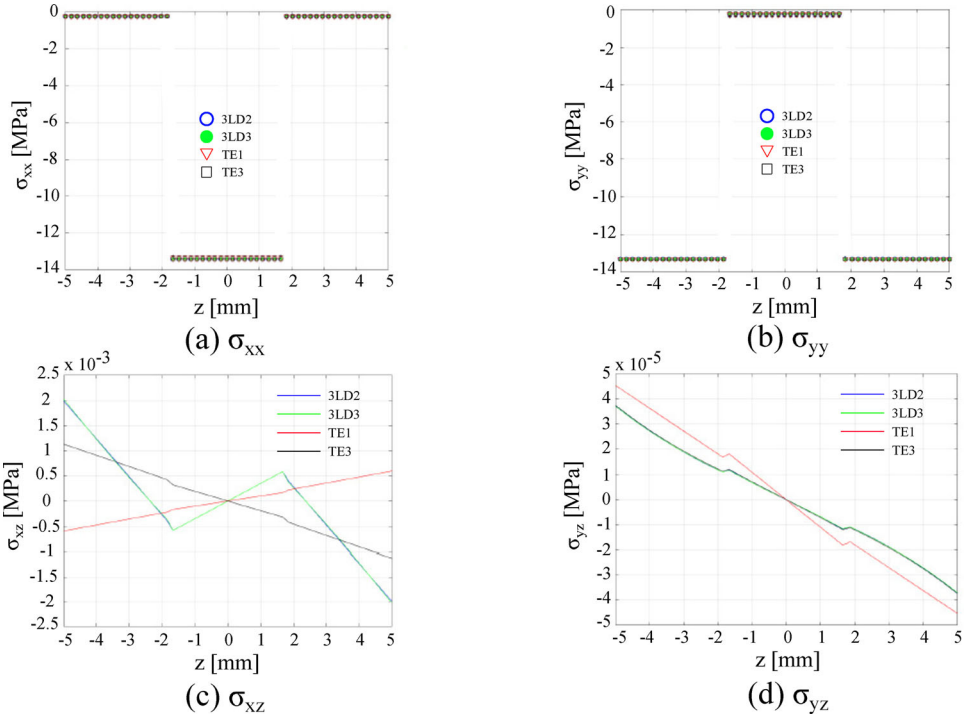

Figure 11. Through-the-thickness stresses distribution for the laminated composite [0°/90°/0°] plate ($a/h = 100$) subjected to $\Delta T = 3\,°C$ at $x = -0.25\,m$ and $y = 0\,m$ considering different kinematic expansions: LD2 (Three-node quadratic Lagrange expansion), LD3 (Four-node cubic Lagrange expansion), TE1 (First-order Taylor-like expansion), TE3 (Third-order Taylor-like expansion).

It can be observed that the frequency of the second vibration mode (2,1) tends to zero at the buckling load value equal to 10.69 °C. Generally speaking, the directionality of the fibers inside the laminate layers determines a variation in the dynamic behavior of thin plates, affecting the buckling. This buckling phenomenon is induced by the state of tension that is generated by the application of thermal loads. For clarity, from the graphs of Figure 11, it can be deduced that the application

Table 5. The first critical buckling load considering different lamination sequences.

Lamination	Buckling mode shape	CUF (°C)	Abaqus (°C)
$[0^\circ/90^\circ/0^\circ]$	Mode (2,1)	10.69	10.42
$[0^\circ/45^\circ/-45^\circ]_s$	Mode (1,1)	11.42	11.30
$[45^\circ/-45^\circ]_s$	Mode (1,1)	9.02	8.91

Laminated composite plate ($a/h = 100$).

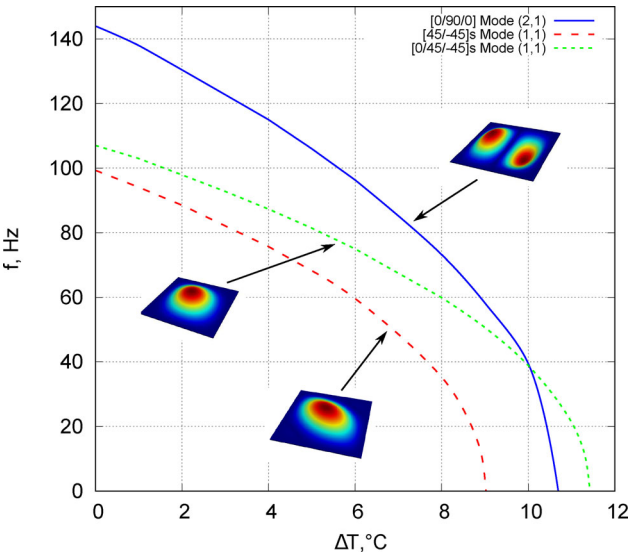

Figure 12. Effect of lamination on the natural frequency variation versus increasing thermal loadings. Laminated composite plate ($a/h = 100$).

of a thermal load due to a uniform variation of the temperature ΔT on the entire laminated structure leads to the generation of compressive stresses. In particular, the stresses σ_{xx} are more intense in the central layer of the laminate, while the stresses σ_{yy} are more intense in the external layers. The structure is consequently subjected to a state of biaxial compression tension. At the critical value of temperature variation ΔT_{cr}, the compressive stresses are able to induce the phenomenon of instability.

Table 5 displays the buckling load values of the composite plates considering different lamination sequences. For the sake of clarity, the numerical results come from simple linearized buckling analyses, where the $\boldsymbol{K}_T$ is approximated as the sum of the linear matrix and the geometric stiffness resulting from the linear stress state. These thermal buckling values are confirmed by the trend of the natural frequencies variation plotted in Figure 12. It is interesting to highlight how the choice of lamination affects the buckling behavior of the structure. In fact, choosing a $[0°/90°/0°]$ lamination causes the variation of the mode shape of the first buckling mode of the plate, passing from a one half-wave, as for the laminations $\left[0^\circ/45^\circ/-45^\circ\right]_s$ and $\left[45^\circ/-45^\circ\right]_s$, to two ones.

In addition, the thickness effect on the frequencies and buckling loads is presented in Figure 13 and Table 6. The results suggest that as the thickness of the laminated composite plate increases, there is a noticeable rising in natural frequencies and critical buckling loads due to the increasing stiffness of the structure.

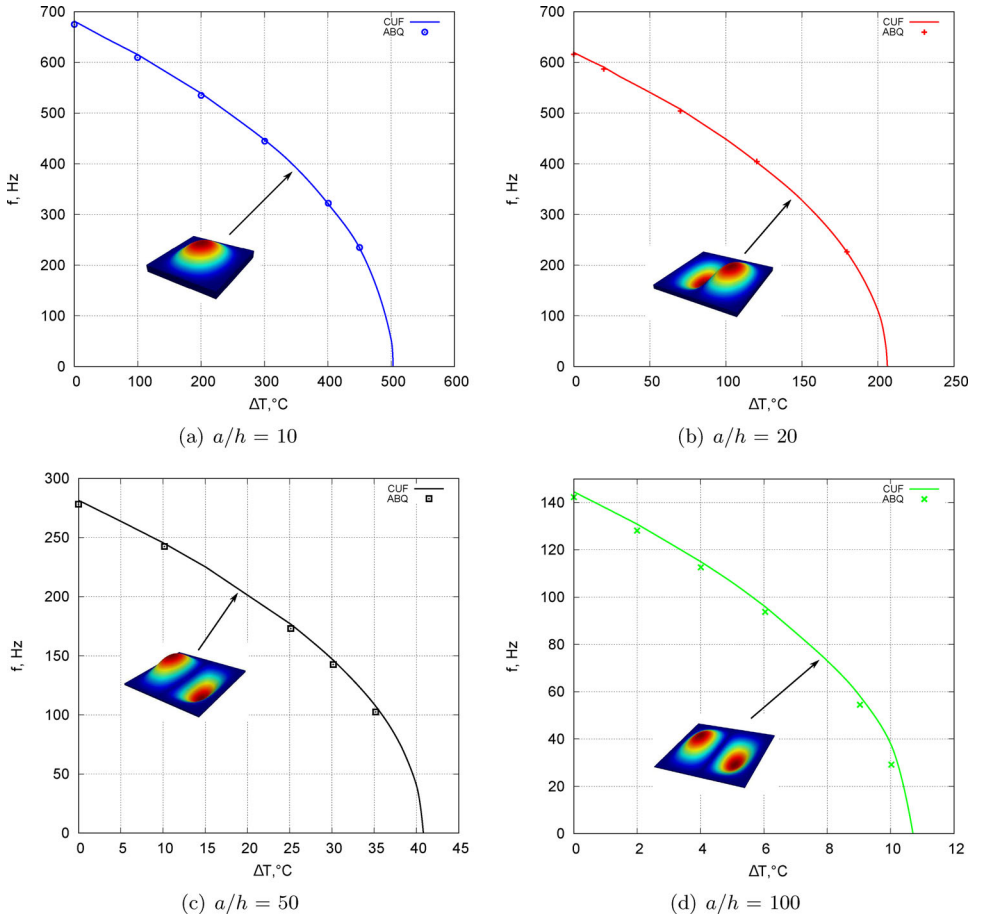

Figure 13. Effect of thickness on the natural frequency variation versus increasing thermal loadings. Laminated composite [0°/90°/0°] plate.

Table 6. The first critical buckling load considering different thickness values of the laminated composite [0°/90°/0°] plate.

a/h	Buckling mode shape	CUF (°C)	Abaqus (°C)
100	Mode (2,1)	10.69	10.42
50	Mode (2,1)	40.80	40.221
20	Mode (2,1)	206.01	206.96
10	Mode (1,1)	502.46	504.60

4. Conclusions

A novel numerical approach to analyze the eigen frequencies and eigen modes of isotropic and laminated composite beam and plate structures subjected to thermal loadings in their quasi-static equilibrium states has been presented in the present research. This methodology allows to predict the critical thermal buckling loads of different structures, investigate the natural frequencies variation for progressively increasing thermal loadings, and provide a verification of the experimental VCT results, which, in some cases, can be difficult to execute. The formulation, based on the CUF, allows one to describe various kinematics models for 1D and 2D isotropic and laminated composite structures. Thus, low- to high-order models can be formulated with ease. The analyses conducted have demonstrated that:

- The proposed approach, in agreement with the solution computed using the software Abaqus, provides a tool able to provide a perfect prediction of critical buckling loads and natural frequencies variation;
- By considering the thermal load and clamped boundary conditions, compressive stresses are generated due to the tendency of the structures to expand as the temperature increases, a tendency which is, however, prevented by the constraint conditions. Therefore, the application of the thermal loadings in this configuration leads to buckling phenomena;
- The choice of the lamination sequence represents a further important variable in the design process of a laminated composite structure that allows or does not respect the imposed design requirements. In fact, changes in the modal form of the first buckling mode are observed for different lamination sequences;
- As the thickness of the laminated composite plate increases, there is a considerable rise in the natural frequencies due to the increasing rigidity of the plate and, therefore, in the thermal buckling load for which the buckling phenomenon occurs.

Future works will concern the vibration-buckling investigation of isotropic, classical composite and variable-angle tow (VAT) beam, plate and shell structures under different distributions of thermal loads by adopting a full nonlinear approach.

Disclosure statement

Authors declare that they have no known competing financial interests or personal relationships that could appear to influence the work reported in this paper.

Funding

This work is part of a project that has received funding from the European Research Council (ERC) under the European Union's Horizon 2020 research and innovation programme (Grant agreement No. 850437).

ORCID

R. Azzara http://orcid.org/0000-0001-5932-3275

References

[1] J. G. Williams and M. Stein, "Buckling behavior and structural efficiency of open-section stiffened composite compression panels," *AIAA J.*, vol. 14, no. 11, pp. 1618–1626, 1976. DOI: 10.2514/3.61497.

[2] S. Y. Kuo, "Flutter of thermally buckled angle-ply laminates with variable fiber spacing," *Compos. Part B: Eng.*, vol. 95, pp. 240–251, 2016. DOI: 10.1016/j.compositesb.2016.04.009.

[3] P. M. Reis, "A perspective on the revival of structural (in) stability with novel opportunities for function: from buckliphobia to buckliphilia," *J. Appl. Mech.*, vol. 82, no. 11, pp. 111001, 2015. DOI: 10.1115/1.4031456.

[4] N. Hu and R. Burgueño, "Buckling-induced smart applications: recent advances and trends," *Smart Mater. Struct.*, vol. 24, no. 6, pp. 063001, 2015. DOI: 10.1088/0964-1726/24/6/063001.

[5] A. R. Champneys, et al., "Happy catastrophe: recent progress in analysis and exploitation of elastic instability," *Front. Appl. Math. Stat.*, vol. 5, pp. 34, 2019. DOI: 10.3389/fams.2019.00034.

[6] J. N. Kotanchik, A. E. Johnson, and R. D. Ross, "Rapid radiant heating tests of multiweb beams," *NACA Tech. Note*, vol. 3474, pp. 1, 1956.

[7] R. R. Heldenfels and W. M. Roberts, *Experimental and Theoretical Determination of Thermal Stresses in a Flat Plate*. Virginia: National Advisory Committee for Aeronautics, Langley Field, 1952.

[8] E. A. Thornton, "Thermal structures: four decades of progress," *J. Aircraft*, vol. 29, no. 3, pp. 485–498, 1992. DOI: 10.2514/3.46187.

[9] J. Gutiérrez Álvarez and C. Bisagni, "A study on thermal buckling and mode jumping of metallic and composite plates," *Aerospace*, vol. 8, no. 2, pp. 56, 2021. DOI: 10.3390/aerospace8020056.
[10] K. Murphy and D. Ferreira, "Thermal buckling of rectangular plates," *Int. J. Solids Struct.*, vol. 38, no. 22–23, pp. 3979–3994, 2001. DOI: 10.1016/S0020-7683(00)00240-7.
[11] R. Javaheri and M. R. Eslami, "Thermal buckling of functionally graded plates," *AIAA J.*, vol. 40, no. 1, pp. 162–169, 2002. DOI: 10.2514/2.1626.
[12] V. Pradeep, N. Ganesan, and K. Bhaskar, "Vibration and thermal buckling of composite sandwich beams with viscoelastic core," *Compos. Struct.*, vol. 81, no. 1, pp. 60–69, 2007. DOI: 10.1016/j.compstruct.2006.05.011.
[13] M. R. Prabhu and R. Dhanaraj, "Thermal buckling of laminated composite plates," *Comput. Struct.*, vol. 53, no. 5, pp. 1193–1204, 1994. DOI: 10.1016/0045-7949(94)90166-X.
[14] V. Bhagat and P. Jeyaraj, "Experimental investigation on buckling strength of cylindrical panel: effect of non-uniform temperature field," *Int. J. Non-Linear Mech.*, vol. 99, pp. 247–257, 2018. DOI: 10.1016/j.ijnonlinmec.2017.12.005.
[15] P. Jeyaraj, "Buckling and free vibration behavior of an isotropic plate under nonuniform thermal load," *Int. J. Struct. Stabil. Dyn.*, vol. 13, no. 03, pp. 1250071, 2013. DOI: 10.1142/S021945541250071X.
[16] L. W. Chen and L. Y. Chen, "Thermal buckling of laminated composite plates," *J. Therm. Stresses*, vol. 10, no. 4, pp. 345–356, 1987. DOI: 10.1080/01495738708927017.
[17] C. A. Meyers and M. W. Hyer, "Thermal buckling and postbuckling of symmetrically laminated composite plates," *J. Therm. Stresses*, vol. 14, no. 4, pp. 519–540, 1991. DOI: 10.1080/01495739108927083.
[18] M. Al-Waily, M. A. Al-Shammari, and M. J. Jweeg, "An analytical investigation of thermal buckling behavior of composite plates reinforced by carbon nano particles," *Eng. J.*, vol. 24, no. 3, pp. 11–21, 2020. DOI: 10.4186/ej.2020.24.3.11.
[19] M. Shariyat, "Thermal buckling analysis of rectangular composite plates with temperature-dependent properties based on a layerwise theory," *Thin-Walled Struct.*, vol. 45, no. 4, pp. 439–452, 2007. DOI: 10.1016/j.tws.2007.03.004.
[20] J. G. Álvarez and C. Bisagni, "Investigation on buckling and mode jumping of composite plates under thermomechanical loads," *Int. J. Non-Linear Mech.*, vol. 138, pp. 103837, 2022. DOI: 10.1016/j.ijnonlinmec.2021.103837.
[21] J. Singer, J. Arbocz, and T. Weller, *Buckling Experiments: Experimental Methods in Buckling of Thin-Walled Structures*, Vol. 1: Basic Concepts, Columns, Beams and Plate. New York, USA: Wiley, 1998.
[22] J. Singer, J. Arbocz, and T. Weller, *Buckling Experiments: Experimental Methods in Buckling of Thin-Walled Structures*, Vol. 2: Shells, Built-up Structures and Additional Topics. New York, USA: Wiley, 2002.
[23] H. Lurie, "Lateral vibrations as related to structural stability," *J. Appl. Mech., ASME*, vol. 19, no. 2, pp. 195–204, 1952. DOI: 10.1115/1.4010446.
[24] J. H. Meier, "The determination of the critical load of a column or stiffened panel in compression by the vibration method," *Proc Soc Exp Stress Anal.*, vol. 11, pp. 1–15, 1953.
[25] T. H. Chu, "Determination of buckling loads by frequency measurements," PhD thesis, California Institute of Technology, California, 1949.
[26] M. A. Souza and L. M. B. Assaid, "A new technique for the prediction of buckling loads from nondestructive vibration tests," *Exp. Mech.*, vol. 31, no. 2, pp. 93–97, 1991. DOI: 10.1007/BF02327558.
[27] M. A. Arbelo, *et al.*, "Vibration Correlation Technique for the estimation of real boundary conditions and buckling load of unstiffened plates and cylindrical shells," *Thin-Walled Struct.*, vol. 79, pp. 119–128, 2014. DOI: 10.1016/j.tws.2014.02.006.
[28] F. Franzoni, *et al.*, "Experimental validation of the Vibration Correlation Technique robustness to predict buckling of unstiffened composite cylindrical shells," *Compos. Struct.*, vol. 224, pp. 111107, 2019. DOI: 10.1016/j.compstruct.2019.111107.
[29] H. Abramovich, *Stability and Vibrations of Thin-Walled Composite Structures*. Duxford, UK: Woodhead Publishing, 2017.
[30] E. Carrera, M. Cinefra, M. Petrolo, and E. Zappino, *Finite Element Analysis of Structures through Unified Formulation*. Chichester, West Sussex, UK: Wiley, 2014,
[31] E. Carrera, A. Pagani and M. Petrolo, "Refined 1D finite elements for the analysis of secondary, primary, and complete civil engineering structures," *J. Struct. Eng.*, vol. 141, no. 4, pp. 04014123/1–14, 2015. DOI: 10.1061/(ASCE)ST.1943-541X.0001076.
[32] A. Pagani, R. Azzara, R. Augello, and E. Carrera, "Stress states in highly flexible thin-walled composite structures by unified shell model," *AIAA J.*, vol. 59, no. 10, pp. 4243–4256, 2021. DOI: 10.2514/1.J060024.
[33] R. Azzara, E. Carrera, M. Filippi, and A. Pagani, "Time response stress analysis of solid and reinforced thin-walled structures by component-wise models," *Int. J. Struct. Stabil. Dyn.*, vol. 20, no. 14, pp. 2043010, 2020. DOI: 10.1142/S0219455420430105.

[34] A. R. Sánchez-Majano, R. Azzara, A. Pagani, and E. Carrera, "Accurate stress analysis of variable angle tow shells by high-order equivalent-single-layer and layer-wise finite element models," *Materials*, vol. 14, no. 21, pp. 6486, 2021. DOI: 10.3390/ma14216486.

[35] E. Carrera, M. Petrolo, M. H. Nagaraj, and M. Delicata, "Evaluation of the influence of voids on 3D representative volume elements of fiber-reinforced polymer composites using CUF micromechanics," *Compos. Struct.*, vol. 254, pp. 112833, 2020. DOI: 10.1016/j.compstruct.2020.112833.

[36] K. J. Bathe, *Finite Element Procedure*. Upper Saddle River, New Jersey, USA: Prentice Hall, 1996.

[37] T. J. R. Hughes, *The Finite Element Method: Linear Static and Dynamic Finite Element Analysis*. Mineola, New York, USA: Courier Corporation, 2012.

[38] E. Carrera and M. Petrolo, "Refined beam elements with only displacement variables and plate/shell capabilities," *Meccanica*, vol. 47, no. 3, pp. 537–556, 2012. DOI: 10.1007/s11012-011-9466-5.

[39] E. Carrera, G. Giunta, P. Nali, and M. Petrolo, "Refined beam elements with arbitrary cross-section geometries," *Comput. Struct.*, vol. 88, no. 5–6, pp. 283–293, 2010. DOI: 10.1016/j.compstruc.2009.11.002.

[40] A. Pagani and E. Carrera, "Unified formulation of geometrically nonlinear refined beam theories," *Mech. Adv. Mater. Struct.*, vol. 25, no. 1, pp. 15–31, 2018. DOI: 10.1080/15376494.2016.1232458.

[41] A. Pagani, R. Augello, and E. Carrera, "Frequency and mode change in the large deflection and post-buckling of compact and thin-walled beams," *J. Sound Vib.*, vol. 432, pp. 88–104, 2018. DOI: 10.1016/j.jsv.2018.06.024.

[42] R. Azzara, E. Carrera, and A. Pagani, "Nonlinear and linearized vibration analysis of plates and shells subjected to compressive loading," *Int. J. Non-Linear Mech.*, vol. 141, pp. 103936, 2022. DOI: 10.1016/j.ijnonlinmec.2022.103936.

[43] J. N. Reddy, "An evaluation of equivalent-single-layer and layerwise theories of composite laminates," *Compos. Struct.*, vol. 25, no. 1–4, pp. 21–35, 1993. DOI: 10.1016/0263-8223(93)90147-I.

[44] E. Carrera, "Multilayered shell theories accounting for layerwise mixed description, part 1: governing equations," *AIAA J.*, vol. 37, no. 9, pp. 1107–1116, 1999. DOI: 10.2514/2.821.

[45] G. Abaqus, *Abaqus 6.11*. Providence, RI, USA: Dassault Systemes Simulia Corporation, 2011.